Volume 4
Number 4
21 February 2023
Pages 979–1204

Materials Advances

rsc.li/materials-advances

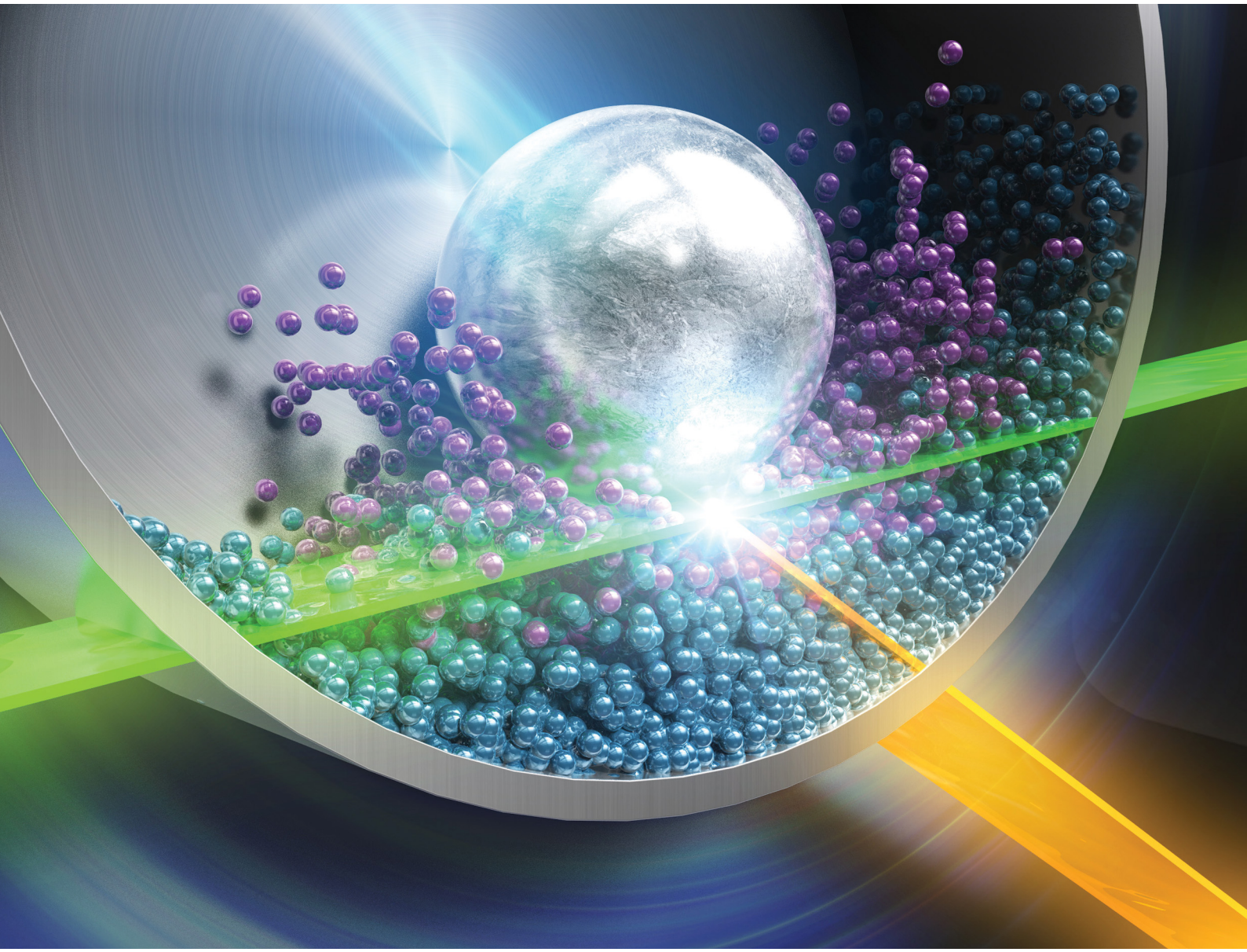

ISSN 2633-5409

ROYAL SOCIETY OF CHEMISTRY

PAPER
Hidetaka Kasai, Eiji Nishibori *et al.*
In situ observation of a mechanically induced self-sustaining reaction for synthesis of silver

Materials Advances

ROYAL SOCIETY OF CHEMISTRY

PAPER

View Article Online
View Journal | View Issue

Cite this: *Mater. Adv.*, 2023, 4, 1005

In situ observation of a mechanically induced self-sustaining reaction for synthesis of silver†

Yanyan Zheng,[a] Hidetaka Kasai, *[a] Shintaro Kobayashi, [b] Shogo Kawaguchi [b] and Eiji Nishibori *[a]

We investigated *in situ* the mechanical reduction of silver chloride with aluminum using synchrotron X-ray diffraction with thermography at SPring-8 BL02B2. A mechanically induced self-sustaining reaction (MSR) was observed for 2 minutes following an activation period of 9 minutes under the present milling conditions. The *in situ* data were analyzed using our developed multi-distance method. The crystal growth of silver was observed from the activation period and was accelerated by the MSR. The growth kinetics induced by the MSR continued for 6 minutes. The *in situ* monitoring clearly distinguished the reaction and crystal growth in the synthesis. We found the two dimensional growth of silver and that reducing the size of silver chloride is dominant in the activation period for the MSR.

Received 15th September 2022,
Accepted 28th December 2022

DOI: 10.1039/d2ma00903j

rsc.li/materials-advances

Introduction

Mechanically induced self-sustaining reactions (MSRs)[1–3] have been used as a solvent-free, direct and energy-efficient synthesis method for the fabrication of functional materials. The MSR is similar to a self-propagating high-temperature synthesis (SHS) reaction,[4] which proceeds by its own heat once it is started. The distinguished feature of MSRs is use of mechanical activation. The MSR occurs in various powder mixtures in which reactions are highly exothermic.[2,3] This includes some of the mechanochemical reduction of silver chloride (AgCl) with metals studied by M. Faraday in the 19th century,[5,6] which sparked scientific studies of mechanochemistry.[7] The reduction is nowadays employed as a synthesis method of fine particles of silver (Ag).[8,9] MSRs have been used for materials synthesis for a variety of applications such as refractories,[10,11] optical devices[12–14] and lithium-ion batteries.[15]

The mechanism of MSRs, especially their activation, has been poorly understood due to their complexity even in the case of AgCl and metal mixtures. Monitoring of the temperature of a container has been extensively used to study processes for MSRs.[2,3,16] This approach has limitations to the observation of MSRs, especially their activation process, and no access to the growth process of products caused by MSRs.

Synchrotron radiation (SR) is the most powerful tool for *in situ* observation of a small amount of sample in a container due to its transmittance, high intensity, tunable wavelength, and controllable beam size. *In situ* monitoring techniques for mechanochemistry using SR powder X-ray diffraction (PXRD) with ball mills have been advanced since the first development by Friščić and coworkers.[17] The advance provides us an opportunity to understand MSRs quantitatively. Emmerling *et al.* combined *in situ* SR-PXRD with thermography to monitor structural evolution and temperature.[18] Michalchuk *et al.* reported a systematic study of kinetics of product formation using *in situ* SR-PXRD.[19]

In situ monitoring of MSR-type synthesis requires detailed data analysis due to the chaotic environment during synthesis. In addition, it is necessary to detect smaller structural changes in the activation period than those in the reaction period. The *in situ* data consist of multiple sample-to-detector distances due to a variety of possible sample positions in a milling container with an inner diameter of ~10 mm. Very recently, Lampronti *et al.* reported the systematic studies with the analytical method which resolved complex diffraction profiles using sample displacement correction.[20]

In the present study, we performed *in situ* SR-PXRD of MSR-type mechanochemical reduction of AgCl with aluminium (Al) at the SPring-8 BL02B2 beamline.[21,22] Firstly, we constructed *in situ* ball mill apparatus. Secondly, we developed an analytical method using the *in situ* data of simple metal powders during ball milling to reveal the structure in MSR processes based on Rietveld refinements. Finally, the processes for MSRs, their activation and crystal growth of Ag were discussed based on a combination of the *in situ* SR-PXRD data and the temperature of the milling jar.

[a] *Department of Physics, Faculty of Pure and Applied Sciences and Tsukuba Research Center for Energy Materials Science (TREMS), University of Tsukuba, 305-8571, Tsukuba, Japan. E-mail: kasai.hidetaka.fw@u.tsukuba.ac.jp, nishibori.eiji.ga@u.tsukuba.ac.jp*

[b] *Diffraction and Scattering Division, Japan Synchrotron Radiation Research Institute (JASRI), 679-5198, Sayo, Japan*

† Electronic supplementary information (ESI) available. See DOI: https://doi.org/10.1039/d2ma00903j

Experimental

Ball milling for *in situ* SR-PXRD

Fig. 1a shows a schematic representation of the experiment carried out at SPring-8 BL02B2.[21,22] The *in situ* setup was used for monitoring an assembly of multiple organic molecules under mechanochemical conditions.[23] *In situ* diffraction data were measured using a flat panel detector (FPD). The sample-to-detector distance was approximately 320 mm. In Fig. 1b, the modified Retsch MM400 mill was installed in the beamline. We modified arms and jar holders on the mill as shown in Fig. S1 (ESI†). The details are shown in the ESI.† The ball mill could be operated at 3–30 Hz. The start and stop buttons of the mill were remotely operated as shown in Fig. S2 (ESI†). The *in situ* setup was prepared on an optical breadboard plate by adjusting the plate position and fixing the mill. We could switch the *in situ* setup to a normal setup, by which automatic data measurement is available using the auto-sampler,[22] within less than an hour. This enabled us to measure the standard data for *in situ* measurements and to evaluate a diffraction profile such as peak asymmetry. In Fig. 1b, an infrared thermography camera, FLIR C5, was used for monitoring the temperature of the jar during *in situ* SR-PXRD measurements for information on the MSR.

We determined the height of the jar for X-ray irradiation with a precision of 0.1 mm by inserting stainless steel spacers between the arm and the holder. We investigated the area near the bottom of the jar, which was the reported strategy for measuring the signal of the sample in between the jar walls with fewer peak splits caused by the signal from the sample adhering to the jar walls.[17] The height of the jar was aligned using the *in situ* data for a jar with milling balls instead of a theodolite.[24] Fig. S3 (ESI†) shows the jar height dependence of the scattered intensity of the milling balls made of agate, *i.e.* SiO_2. The intensity from the balls decreased as the X-ray irradiation position went down against the jar.

Materials

Al (Kojundo Chemical Lab., 99.9% purity), Ni (Mitsuwa Chemicals, 99.9% purity), and AgCl (FUJIFILM Wako Pure Chemical Corporation, >99.5% purity) were used as samples. Al and Ni powders consist of fine particles with a size of micrometers. The as-received AgCl powder consists of various sized aggregates. The AgCl aggregates were weighed and flattened to millimeter-sized thickness just before ball milling.

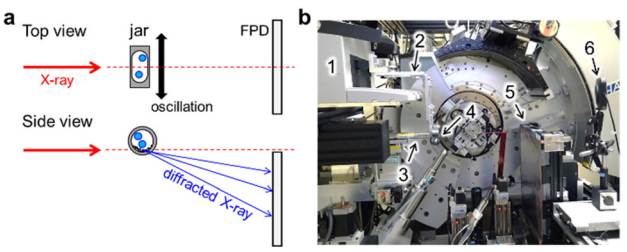

Fig. 1 Ball mill installed at SPring-8 BL02B2 for *in situ* SR-PXRD measurements. (a) Schematic of the experimental setup. (b) Side-view photograph. 1: Retsch MM400 mill, 2: arm and holder, 3: collimator, 4: milling jar, 5: flat panel detector (FPD), and 6: infrared thermography camera.

In situ and *ex situ* measurements

We used the modified Retsch MM400 for both *in situ* and *ex situ* measurements. Ball milling was conducted with a 3D-printed milling jar[25] as shown in Fig. S4 (ESI†), agate balls with a diameter of 3 mm or 5 mm, and mill operation at 20 Hz. The details of our jar are provided in the ESI.† Plastic jars were not reused. We performed *in situ* SR-PXRD during ball milling at SPring-8 BL02B2.[21,22] The wavelengths of incident X-rays were calibrated using the NIST CeO_2 standard powder, the diffraction data of which were measured using both the FPD and multiple MYTHEN detectors. The X-ray beam was collimated to 0.5 mm in height and 3.0 mm in width. The FPD with a pixel size of 100 μm, Varex Imaging XRD3025, was used for *in situ* data collection with an exposure time of 1 or 2 s. The data with a time resolution of one minute were prepared for analysis by summing 60 and 30 data frames with exposure times of 1 s and 2 s, respectively.

Ball milling of Al and Ni

The amount of powder loaded in the jars made of polylactic acid (PLA) was 150 mg for ball milling Al and Ni powders. We performed *in situ* SR-PXRD during ball milling of the metal powder. The wavelengths of incident X-rays were 0.500 Å and 0.328 Å for Al and Ni, respectively. SR-PXRD data of both the unmilled samples in glass capillaries were also collected using a large Debye–Scherrer camera with an imaging plate (IP) as a detector to determine the lattice parameters before milling.

Mechanochemical reduction of AgCl with Al

We performed four kinds of experiments: (i) *ex situ* experiments at the laboratory, (ii) *in situ* SR-PXRD, (iii) *in situ* SR-PXRD with only AgCl, and (iv) PXRD of the product after (ii) at the laboratory. A polycarbonate (PC) jar with an inner diameter (ID) of 12 mm and four balls with a diameter of 3 mm were used for all the ball milling experiments. The wavelength of incident X-rays was 0.700 Å for (ii and iii). A SmartLab diffractometer with Mo Kα radiation was used at a scan rate of 1° min^{-1} for (i and iv).

We conducted *ex situ* experiments to determine milling conditions for *in situ* SR-PXRD measurements in (i). The charged amounts were 400 mg and 30 mg for AgCl and Al, respectively. 20% more Al than stoichiometry was loaded in order to compensate for the partial oxidation of aluminum.[6] Ball milling was conducted by monitoring the temperature by thermography. After we performed ball milling for 30 minutes, the jar was opened and the product and balls were removed from the jar. The micrometer-sized particles in the product were covered by tape within 20 minutes after ball milling. We measured PXRD of the product from 24 minutes after ball milling.

The milling conditions determined in (i) were used for *in situ* measurements. The samples were weighed and loaded into the PC jar with the balls at the beamline. We performed

the *in situ* SR-PXRD measurements during ball milling for 30 minutes. The jar was opened and the balls were removed after the measurements. In (iii), we performed *in situ* SR-PXRD for ball milling of AgCl. The charged amount of AgCl was 400 mg. The other conditions were the same as in (ii).

In (iv), we measured PXRD of the product of (ii). The jar was opened again 12 days after (ii). There were fine particles with micrometer size and millimeter-sized aggregates which were removed easily from the jar and fine particles adhering to the jar wall. The particles with different sizes were covered by tape and characterized by PXRD at the laboratory.

Results and discussion

Multi-distance method for *in situ* data analysis

We developed an analytical method using the SR-PXRD patterns of Al and Ni powders during milling. For these simple metals, it was possible to eliminate peak asymmetry by the instrumental effect for all the observed reflections due to the diffraction angle $2\theta_{hkl}$ of more than 9°. The complex shape of Bragg reflections was attributed to the peak splitting by sample distribution on the X-ray beam path.[20] The high-resolution SPring-8 data enabled us to observe fine details in between the peaks as shown in Fig. S5 (ESI†). We tried to analyze this complex profile using the already reported methods using multiple phases with different lattice constants[17] and two split-type pseudo-Voigt functions plus one Gaussian function.[20] However, these techniques have some insufficient points for the analysis of the present high-resolution data especially at the peaks in between the two peaks from the front and back walls of the jar.

Fig. 2 schematically shows our developed method. The scattering angle $2\theta_i$ for the ith sample position, *i.e.* sample-to-detector distance L_i, is expressed by

$$2\theta_i = \arctan\left[0.1\cdot(x - x_0)/L_i\right] \quad (1)$$

where x is the pixel number of FPD, x_0 is the position of the direct beam in terms of the pixel number and L_i is in terms of mm. The representative 2θ was transformed from the FPD pixel number using a reference sample-to-detector distance L_0 and the estimated x_0. In the analysis, the ith powder profile was calculated using L_i and L_0 against the representative 2θ. We determined the L_i value with the refinements. The discrepancy in x_0 was treated by a zero-shift parameter.

The method is similar to the strategy reported by Lampronti *et al.*[20] The differences of our method for the peak splitting are that (1) more than three calculated profiles are available and (2) all the profiles are assumed as split-type pseudo-Voigt functions. We provided all of the profile parameters for each profile. The flexibility of our method enables us to analyze the complex shape of powder profiles as shown in Fig. S5 (ESI†). We call this technique a multi-distance method. The multi-distance method was implemented in the synchrotron powder (SP) program.[26]

The multi-distance method achieved the satisfactory fitting in the 2θ range of up to 40° in Fig. 3, Fig. S6 and S7 (ESI†). Reliability factors based on the weighted profiles, R_{wp}, and on the intensity, R_I, are 0.77% and 2.47% for Al, and 1.57% and 2.71% for Ni, respectively. The details of refinements are given in the ESI.† The number of sample-to-detector distances was determined to be a minimum value which achieves the smallest R_{wp} by trial refinements by changing the number. The R_{wp} decreased and became almost constant with an increasing number of sample-to-detector distances in Fig. S8 (ESI†). The data were fitted by the four profiles of Al with the sample-to-detector distances of L_1: 323.8 mm, L_2: 325.5 mm, L_3: 328.1 mm and L_4: 330.8 mm with an accuracy of approximately ± 0.1 mm

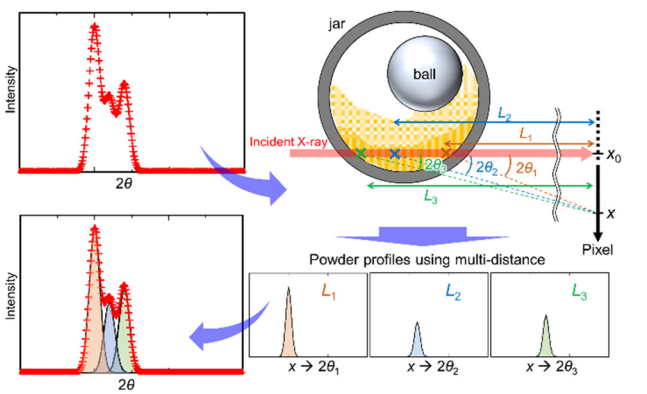

Fig. 2 Multi-distance method for *in situ* SR-PXRD data during ball milling. The powder profiles with multiple sample positions are treated as a sum of those with each sample-to-detector distance.

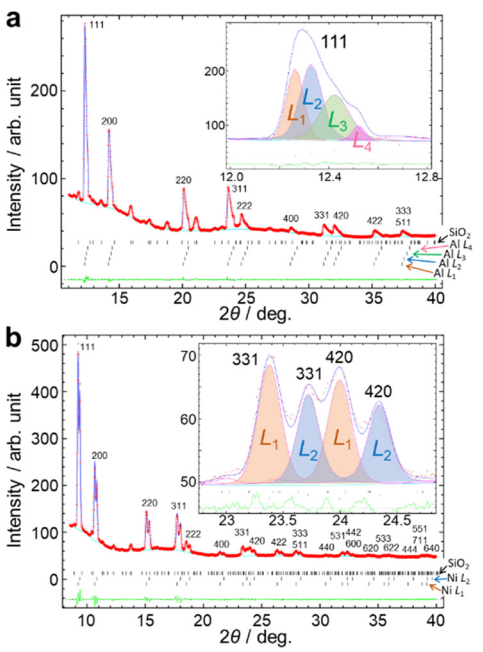

Fig. 3 Fitting results of Rietveld refinement using the multi-distance method for the *in situ* SR-PXRD data for (a) Al and (b) Ni. (a) 0–1 min using a jar of ID: 12 mm and four balls with a diameter of 5 mm. (b) 29–30 min using a jar of ID: 10 mm and two balls with a diameter of 5 mm. (a and b) Red points, blue lines, light blue lines, green lines, and black bars represent observed, calculated, background and difference intensities, and positions of Bragg reflections, respectively.

using the identical lattice parameter. In Fig. 3b, the multi-distance method used the two sample-to-detector distances of L_1: 325.7 mm and L_2: 331.0 mm for Ni.

The *in situ* diffraction pattern in Fig. 3a shows a sum of the four profiles resulting in more complex peak shapes than the reported *in situ* data using a jar with an ID of 10 mm.[20] The difference can be attributed to the sample distribution, the length of which is more than 7.0 mm calculated from L_1 and L_4 in Fig. 3a. The L_1 and L_4 were attributed to the sample positions close to the front and back walls of the jar.[20] The L_2 and L_3 correspond to the in-between positions. The peak widths for the in-between positions were larger than those for the front and back walls. The width of the 511 reflection for the in-between positions was $\sim 0.3^\circ$ by projection of 3 mm for an irradiated area of the sample.

In situ monitoring of the mechanochemical reduction of AgCl with Al

We applied our *in situ* apparatus and multi-distance method to the mechanochemical reduction of AgCl with Al. The reaction equation is described as

$$3AgCl + Al \rightarrow 3Ag + AlCl_3 \quad (2)$$

This reaction is exothermic with the ratio of the reaction heat to the RT heat capacity of the products $\Delta H/C$ of 1933 K.[6] The $\Delta H/C$ is much higher than the sublimation temperature 453 K of $AlCl_3$. The reduction was reported as an MSR.[6]

We confirmed the synthesis of Ag using the modified mill and the milling conditions in Experiment (i). Fig. 4 shows the PXRD pattern of the reaction product. It confirmed that Ag was synthesized using the hexahydrate form of $AlCl_3$. The growth of $AlCl_3{\cdot}6H_2O$ occurred from saturated aqueous solution of $AlCl_3$ by air moisture.[27]

The temperature of a milling jar is an indicator of ignition of the MSR. Fig. 4 also shows the thermography images during ball milling in Experiment (i). The temperature increased drastically at a milling time of 10 minutes, indicating ignition of the MSR. Subsequently, the temperature decreased to its original within 2 minutes, indicating that the MSR and the deceleration periods were completed.

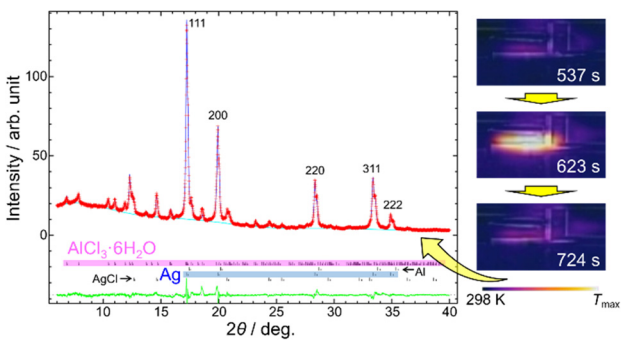

Fig. 4 PXRD pattern of the product and thermography images of the jar during ball milling. A color bar indicates temperature, of which the maximum T_{max} values are 313 K and 310 K for 623 s and others, respectively.

The process of the mechanochemical reduction was monitored by *in situ* SR-PXRD in Experiment (ii). Fig. 5, Fig. S9 and S10 (ESI†) show the *in situ* diffraction data and monitored temperatures. We observed the growth of Ag in the figures. The time change of temperature of the jar in Fig. 5a is consistent with that in Fig. 4. Fig. S11 (ESI†) shows the micrometer-sized particles obtained by the mechanochemical reduction.

The size reduction of AgCl by ball milling caused the increase of its micrometer-sized particles. The increase of AgCl was observed until 9 minutes and after 11 minutes in Fig. 5a, Fig. S8 and S9 (ESI†). *In situ* SR-PXRD for ball milling of only AgCl was carried out in Experiment (iii) and the pattern is shown in Fig. S12 (ESI†). The pattern confirmed the increase of the amount for micrometer-sized AgCl particles.

The millimeter-sized AgCl aggregates did not react. In other words, the reaction occurred for the fine particles with micrometer size of AgCl. The PXRD data of the product with different sizes were collected in Experiment (iv). The patterns showed that the ratio of the amount for AgCl was higher in the millimeter-sized aggregates than that in the micrometer-sized particles as shown in Fig. S13 (ESI†).

The *in situ* diffraction patterns clearly show the peak splitting due to sample distribution on the beam path as shown in Fig. 5b, Fig. S9 and S10 (ESI†). The weak signal from the balls confirmed the alignment of the X-ray beam across the nearly shortest path length near the bottom of the jar. We observed at least three components for each of AgCl, Al and Ag. Fig. 5b and Fig. S10 (ESI†) show the fitting results of Rietveld refinements using the multi-distance method. The profile was fitted with three sample-to-detector distances of 323.0 mm, 328.6 mm and 332.3 mm for the materials. There were Ag 200, Al 200 and AgCl 220 reflections with each splitting, *i.e.* total of nine components, around 2θ = 20–21° as shown in Fig. S10 (ESI†). The complex profile was successfully resolved by the multi-distance method in the figure.

Fig. 5 shows the time evolution of the relative amount of the reactants and product. The scale factors from the three sample-to-detector distances were summed and normalized for each material in the figure. The time evolution of AgCl confirmed the above-mentioned size reduction process and the MSR from 9 to 11 minutes in Fig. 5a. Al decreased within two minutes in the figure. This was attributed to sample spreading, also observed in Fig. S5 (ESI†). Ag increased slowly until 9 minutes and subsequently drastically from 9 to 15 minutes as shown in Fig. 5b.

The MSR occurred for 2 minutes after an activation time of 9 minutes under the present conditions. This was confirmed by the changes of AgCl and the temperature of the jar. The size reduction of AgCl was a dominant process in the activation period. The reaction occurred slightly even in the activation period. The onset of the drastic growth of Ag is consistent with the ignition of the MSR. $AlCl_3{\cdot}6H_2O$ was not observed in the *in situ* data. This fact indicates that the crystal growth of

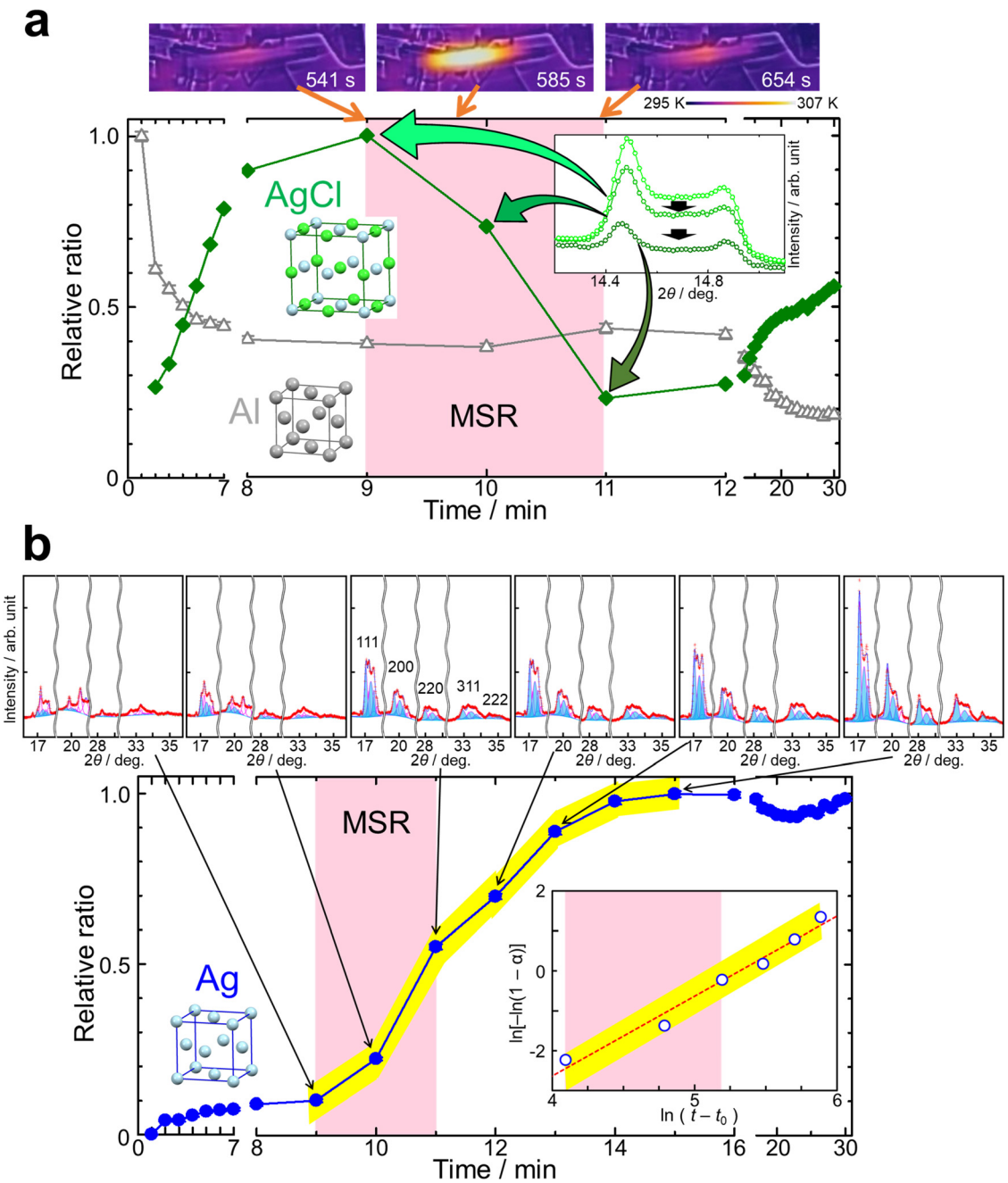

Fig. 5 Time evolution of the relative amount for (a) reactants and (b) product. The scale factors from Rietveld refinements were normalized by the maximum values for each material. The insets represent thermography images, diffraction patterns for the 200 reflection of AgCl, fitting results for reflections of the metals, crystal structures, and Avrami plot for the growth of Ag with a linear fit.

$AlCl_3 \cdot 6H_2O$ occurred after ball milling. The MSR was terminated probably due to an insufficient amount of the fine particles of AgCl as shown in Fig. 5a. It was not investigated whether the MSR re-occurs or not after 30 minutes by re-increasing the amount of fine particles of AgCl by size reduction after 11 minutes in this study.

We observed the growth of Ag even after the MSR was completed including its deceleration period in Fig. 5b. The figure also shows the Avrami plot for the growth of Ag. The crystallization kinetics was described by the Kolmogorov–Johnson–Mehl–Avrami (KJMA) model: $\alpha(t) = 1 - \exp[-k(t - t_0)^n]$, where α is the relative ratio of the product, t is the ball milling time, t_0 is the induction time, k is the crystallization rate constant, and n is a kinetic exponent. The kinetics after the ignition of the MSR was described with t_0 of 480 s, $n = 2.00(3)$ and $\ln(k) = -10.63(16)$, indicating the same growth mechanism from 9 to 14 minutes. The n value of 2 indicates two or one dimensional crystal growth. Two dimensional crystal growth was supported by the preferable growth in the 111 direction indicated by the peak widths in the diffraction data.

The *in situ* SR-PXRD and the data analysis unveiled the activation, MSR, and crystal growth processes. The MSR was ignited by increasing micrometer-sized particles of AgCl, which took 9 minutes. The MSR accelerated the growth of the product and continued for 2 minutes. The decrease of fine particles of AgCl for 2 minutes was associated with the MSR due to consumption by the reaction. The MSR resulted in the change of the kinetics for Ag. The growth of Ag continued with the kinetics caused by the MSR for 6 minutes, which was longer than the reaction. This is due to the growth processes such as diffusion, nucleation and crystal growth following the reaction. The kinetics and the diffraction data indicated two dimensional crystal growth.

Conclusions

We revealed the processes for the MSR-type synthesis of Ag particles. The processes were described by activation, MSR and crystal growth of Ag. The activation process was dominated by making micrometer-sized AgCl particles as observed by *in situ* SR-PXRD. The MSR and the decelerated reaction were completed before the crystal growth of Ag was saturated. This showed that the chemical reaction and crystal growth are different steps, which are distinguished by *in situ* SR-PXRD. The multi-distance method suggests that detailed *in situ* monitoring can be carried out for various positions in a milling jar. We believe that our *in situ* apparatus and multi-distance method will reveal processes of a variety of mechanochemical reactions, resulting in the advancement in science for materials synthesis.

Conflicts of interest

There are no conflicts to declare.

Acknowledgements

This work was supported by JSPS KAKENHI Grant Numbers JP19KK0132, JP20H04656 and JP21H05235. The synchrotron experiments were performed at SPring-8 BL02B2 with the approval of the Japan Synchrotron Radiation Research Institute (JASRI) (Proposal No. 2021A0068 as a Partner User and Proposal No. 2021B1630, 2021B1775, 2021B1783, 2022A1231 and 2022A1754).

Notes and references

1 C. G. Tschakarov, G. G. Gospodinov and Z. Bontschev, *J. Solid State Chem.*, 1982, **41**, 244.
2 L. Takacs, *Prog. Mater. Sci.*, 2002, **47**, 355.
3 L. Takacs, *Int. J. Self-Propag. High-Temp. Synth.*, 2009, **18**, 276.
4 J. J. Moore and H. J. Feng, *Prog. Mater. Sci.*, 1995, **39**, 243.
5 M. Faraday, *Q. J. Sci., Lit., Arts*, 1820, **8**, 374.
6 L. Takacs, *J. Therm. Anal. Calorim.*, 2007, **90**, 81.
7 L. Takacs, *Chem. Soc. Rev.*, 2013, **42**, 7649.
8 J. Keskinen, P. Ruuskanen, M. Karttunen and S. P. Hannula, *Appl. Organomet. Chem.*, 2001, **15**, 393.
9 M. T. Le, D. J. Kim, C. G. Kim, J. S. Sohn and J. Lee, *J. Exp. Nanosci.*, 2008, **3**, 223.
10 M. Jalaly, F. J. Gotor and M. J. Sayagués, *J. Am. Ceram. Soc.*, 2018, **101**, 1412.
11 S. Eilbeigi, S. A. Hassanzadeh-Tabrizi and A. Khodaivandi, *Ceram. Int.*, 2018, **44**, 21437.
12 M. A. Avilés, J. M. Córdoba, M. J. Sayagués and F. J. Gotor, *Inorg. Chem.*, 2019, **58**, 2565.
13 M. A. Avilés, J. M. Córdoba, M. J. Sayagués and F. J. Gotor, *J. Mater. Sci.*, 2020, **55**, 1603.
14 M. A. Avilés and F. J. Gotor, *Opt. Mater.*, 2021, **117**, 111121.
15 Ö. Budak, P. Srimuk, M. Aslan, H. Shim, L. Borchardt and V. Presser, *ChemSusChem*, 2021, **14**, 398.
16 J. M. Pauls, N. F. Shkodich and A. S. Mukasyan, *J. Phys. Chem. C*, 2019, **123**, 11273.
17 T. Friščić, I. Halasz, P. J. Beldon, A. M. Belenguer, F. Adams, S. A. J. Kimber, V. Honkimäki and R. E. Dinnebier, *Nat. Chem.*, 2013, **5**, 66.
18 H. Kulla, S. Haferkamp, I. Akhmetova, M. Röllig, C. Maierhofer, K. Rademann and F. Emmerling, *Angew. Chem., Int. Ed.*, 2018, **57**, 5930.
19 A. A. L. Michalchuk, I. A. Tumanov, S. Konar, S. A. J. Kimber, C. R. Pulham and E. V. Boldyreva, *Adv. Sci.*, 2017, **4**, 1700132.
20 G. I. Lampronti, A. A. L. Michalchuk, P. P. Mazzeo, A. M. Belenguer, J. K. M. Sanders, A. Bacchi and F. Emmerling, *Nat. Commun.*, 2021, **12**, 6134.
21 E. Nishibori, M. Takata, K. Kato, M. Sakata, Y. Kubota, S. Aoyagi, Y. Kuroiwa, M. Yamakata and N. Ikeda, *Nucl. Instrum. Methods Phys. Res., Sect. A*, 2001, **467**, 1045.
22 S. Kawaguchi, M. Takemoto, K. Osaka, E. Nishibori, C. Moriyoshi, Y. Kuroiwa and K. Sugimoto, *Rev. Sci. Instrum.*, 2017, **88**, 085111.
23 Y. Yano, H. Kasai, Y. Zheng, E. Nishibori, Y. Hisaeda and T. Ono, *Angew. Chem., Int. Ed.*, 2022, **61**, e20223853.
24 I. Halasz, S. A. J. Kimber, P. J. Beldon, A. M. Belenguer, F. Adams, V. Honkimäki, R. C. Nightingale, R. E. Dinnebier and T. Friščić, *Nat. Protoc.*, 2013, **8**, 1718.
25 N. Tumanov, V. Ban, A. Poulain and Y. Filinchuk, *J. Appl. Crystallogr.*, 2017, **50**, 994.
26 E. Nishibori, E. Sunaoshi, A. Yoshida, S. Aoyagi, K. Kato, M. Takata and M. Sakata, *Acta Crystallogr., Sect. A: Found. Crystallogr.*, 2007, **63**, 43.
27 D. R. Buchanan and P. M. Harris, *Acta Crystallogr., Sect. B: Struct. Crystallogr. Cryst. Chem.*, 1968, **24**, 954.